LAWRENCE
LIVERMORE
NATIONAL
LABORATORY

UCRL-PROC-208355

Integrated laser with low-loss high index-contrast waveguides for OEICs

R. J. Welty, T. C. Bond, E. Behymer, M. Pocha, G. Loomis, J. Wolfe, S. Vernon

December 2, 2004

SPIE, International Symposium on Integrated Optoelectronic Devices
San Jose, CA, United States
January 22, 2005 through January 27, 2005

Integrated laser with low-loss high index-contrast waveguides for OEICs

R.J. Welty, T.C. Bond, E. Behymer M. Pocha, G. Loomis, J. Wolfe, S. Vernon
Center for Micro and Nano Technology,
Lawrence Livermore National Laboratory, Livermore, CA.

Photonic integrated circuits require the ability to integrate both lasers and waveguides with low absorption and coupling loss. This technology is being developed at LLNL for digital logic gates for optical key generation circuits to facilitate secure communications. Here, we demonstrate an approach of integrating InGaAs DQW edge emitting lasers (EEL) with electron beam evaporated dielectric waveguides. The EELs are defined by electron cyclotron resonance etching (ECR). This approach results in highly anisotropic etched mirrors with smooth etched features (sidewall rms roughness = 28 Å, surface rms roughness = 10 Å). The mirror is etched to form both the laser cavity and define the waveguide mesa, which accommodates a dielectric stack, where the core is aligned with the active region of the laser to achieve maximum vertical mode overlapping. The waveguides are based on $SiO_2/Ta_2O_5/SiO_2$ which yields a high index contrast of 0.6, resulting in low loss guides (~2-3dB/cm). The design of the interface has taken into account the waveguide transmission loss, air gap spacing and tilt between the laser and waveguide. The critical feature for this deposition technique is its required high directionality or minimal sidewall deposition and corner effects. In the butt coupled EEL/waveguide system we have measured a slope efficiency to be as high as 0.45 W/A. We have in conclusion demonstrated a technology that allows direct coupling of a dielectric optical interconnect to a semiconductor laser monolithically fabricated on the semiconductor substrate.

Keywords: Photonic integrated circuits, electron cyclotron resonance (ECR) etching, dielectric waveguides, edge emitting laser, etched facet

1. INTRODUCTION

There is a continuing interest in the development of high speed all optical communication systems for applications in both high speed [1] and secure communications [2]. Monolithic integration of the devices needed to implement such a system is still in development. In order to have a complete device family capable of providing the necessary requirements one needs to be able to generate, route, amplify and switch signals. In order to satisfy all of these requirements it is desirable to integrate lasers and waveguides on a single wafer. There have been many approaches to solve this problem which are generally either done by modifying the substrate wafer or by adding another material to the host wafer in order to create a region with a different bandgap energy. In the substrate modification approach, there is active research in quantum well intermixing [3], in this approach the area of the wafer that will guide light is shifted in wavelength from the laser portion, this can be done by material modification via thermal processing with selective capping layers [3]. Other approaches that can be taken include using an alternate material for the waveguiding region, such as SiO_2, polyimide [4], or semiconductors which are generally done by sputtering, evaporation, spin-on processes or regrowth. Another approach is hybrid integration which involves bonding of dissimilar substrates [5]. Here we present an approach to integrate quantum well lasers with dielectric waveguides on a GaAs substrate. These lasers have etched facets which lend themselves well to integration in a planar configuration. The basic design of the DQW lasers and waveguides is shown with emphasis on the determination of the process parameters done by computation of the optical beam mode alignment in the laser and waveguide. This was done using both the BeamProp package by RSoft Inc. and codes developed at LLNL. The integrated waveguide and laser is the building block device for an optical integrated circuit which due to its planar configuration can be readily integrated with turning mirrors, and beamsplitters for further signal routing and functionality.

2. DQW LASER AND DIELECTRIC WAVEGUIDES

The basic configuration for the integrated laser and waveguide is shown in Figure 1. We are aligning in the vertical direction a DQW InGaAs etched facet laser with a dielectric waveguide. The device is processed to have the optical mode in the laser match up with the core region of the waveguide. With this approach a low loss circuit is possible.

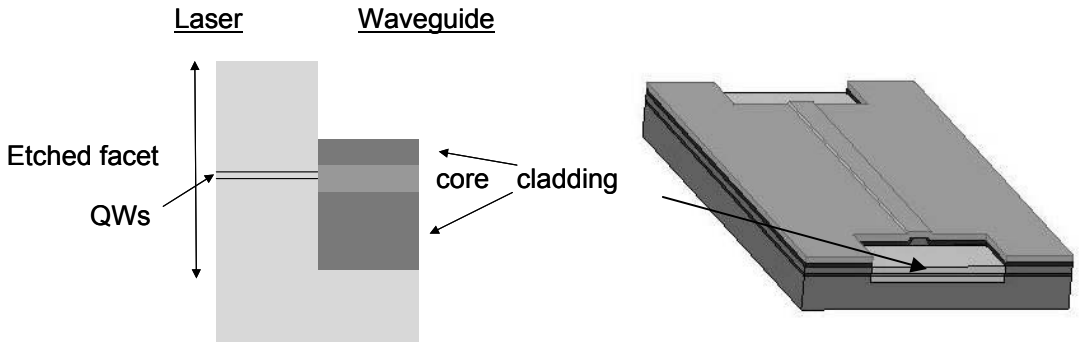

(a) (b)

Figure 1 (a) Sketch of integrated DQW etched facet edge-emitting laser with a dielectric waveguide. (b) The dielectric waveguide stack is deposited in an etched mesa.

Table 1 shows the epilayer design of the DQW laser. The laser is grown on an n+ GaAs substrate, has AlGaAs cladding layers and InGaAs quantum wells. The laser operates at 950-970 nm (function of applied current) and from characterization of cleaved facet lasers has the following figures of merits: $\eta_i \sim 0.8$, $J_{tr} < 200$ A/cm^2 and $\alpha \sim 11$ cm^{-1} (data extraction was done with a set of lasers with the following lengths 300, 500, 700, 900 μm).

Table 1 Epilayer design for double quantum well laser grown on a GaAs substrate.

Layer #	Material Type	Alloy (x,y)	T (μm)	Doping (cm-3)	Type	Dopant
16	GaAs		0.02	1.6E+19	p+	Zn
15	GaAs		0.18	1.7E+18	p	Zn
14	Al(x)GaAs	0.2	0.20	2.0E+18	p	Zn
13	Al(x)GaAs	0.6->0.2	0.20	0.3>2E+18	p	Zn
12	Al(x)GaAs	0.6	1.00	2.8E+17	p	Zn
11	Al(x)GaAs	0.11->0.6	0.20	-	UD	-
10	Al(x)GaAs	0.11	0.01	-	UD	-
9	GaIn(y)As	0.11	~0.0115	-	UD	-
8	Al(x)GaAs	0.11	0.015	-	UD	-
7	GaIn(y)As	0.10	~0.0115	-	UD	-
6	Al(x)GaAs	0.11	0.01	-	UD	-
5	Al(x)GaAs	0.6->0.11	0.20	5e16>3e17	n	Si
4	Al(x)GaAs	0.6	1.00	2.0E+17	n	Si
3	Al(x)GaAs	0.2->0.6	0.20	2e17>2e18	n	Si
2	Al(x)GaAs	0.2	0.20	2.0E+18	n	Si
1	GaAs		0.25	2.0E+18	n	Si
	n+ GaAs Substrate					

We first analyzed the vertical waveguide to initially define the slab design that would offer the best vertical mode overlap between the laser and waveguide modes. The waveguide design is shown in Table 2. The core region of the waveguide is tantalum pentoxide and is clad by regions of silicon dioxide. The design was based on having a highly confined mode such that the absorbing GaAs substrate is optically invisible. This is achieved by having the bottom cladding thickness at 1.2 μm. If this layer is reduced there will be a penalty in loss. The core of the waveguide was

determined to provide single mode behavior. The top cladding layer is chosen to provide additional optical confinement. Details of the waveguide mode are shown in Figure 2. Figure 2a shows that the mode is tightly confined and results in an ideal (no scattering) loss of ~ 0.5 dB/cm. Figure 2b shows that the waveguide is single mode. Our integrated system requires that both the waveguide and laser be single mode to have low loss interconnects.

Table 2 Dielectric slab waveguide design. Refractive index measured done by a Carey Spectrophotmeter, the index is shown at $\lambda = 950$ nm.

Layer #	Material Type	Index	T (μm)
3	SiO_2	1.435	0.5
2	Ta_2O_5	2.103	0.12
1	SiO_2	1.435	1.2
	n+ GaAs Substrate	3.54	

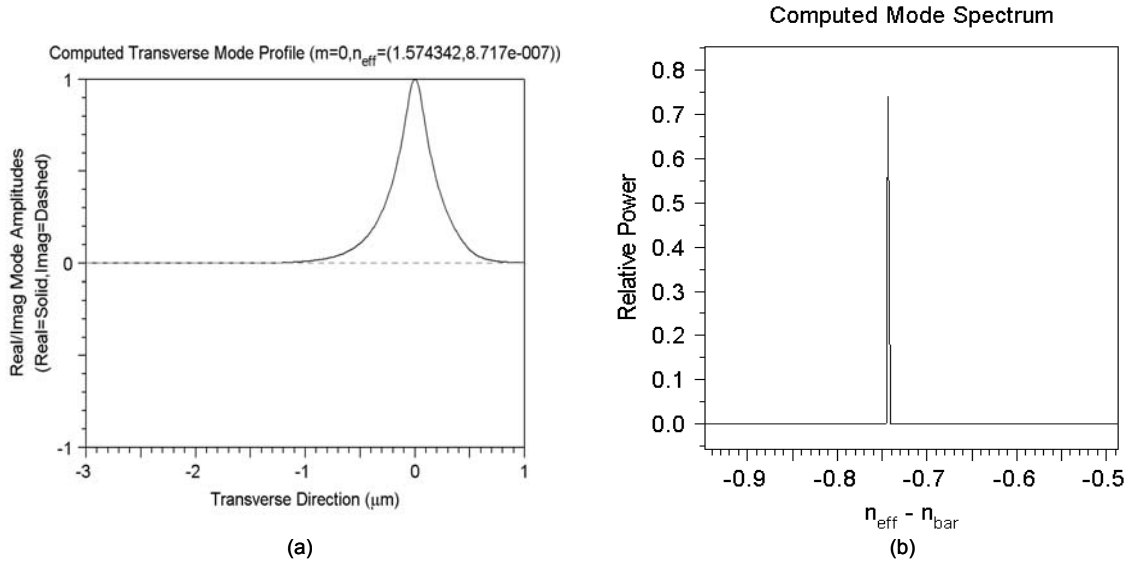

Figure 2 (a) Simulated mode amplitude and (b) spectrum for device waveguide shown in Table 2. Intrinsic loss of ~ 0.5 dB/cm is derived and single mode behavior is shown.

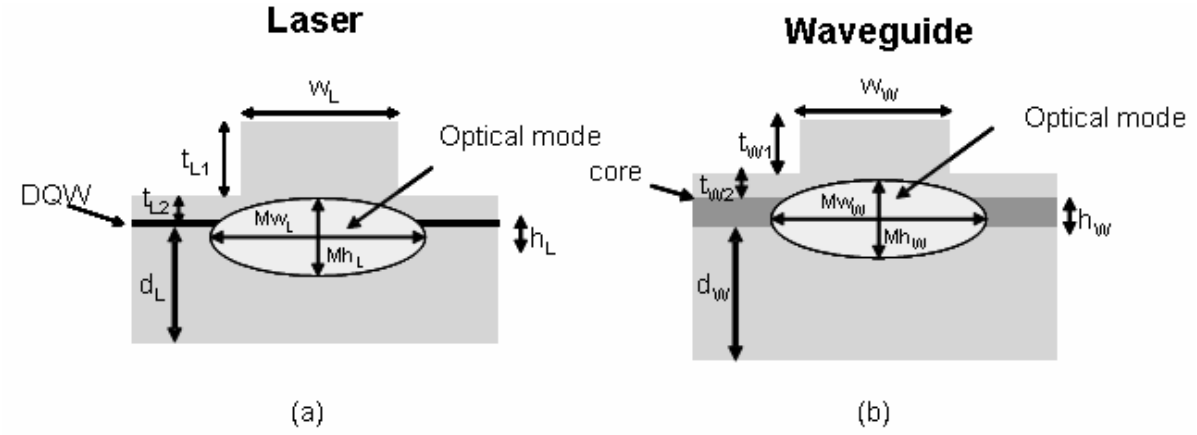

Figure 3 Sketches of the etch profile and mode size for (a) the laser and (b) waveguide.

In order to increase the confinement of the mode in both the laser and the waveguide, a mesa etch is done to increase the index contrast. This is schematically shown in Figure 3 where the geometrical dimensions used in the following discussion are defined. In order to have a low loss interface between the laser and the waveguide the mode in both devices should be matched in both the width and height. We approached this problem with a 3D solver to analyze and design the ridge semiconductor laser and oxide waveguides for best coupling.

We first looked at the effect of the laser ridge widths and etched depths on the mode widths and heights. In Figure 4 we show the effect of the width of the laser ridge w_L and ridge etch depth t_{L1} on the fundamental mode width Mw_L and height Mh_L for the ridge laser (Table 1). Values are summarized in Table 3 for convenience. The range of values [1.5 μm, 1.7 μm] for the ridge etch t_{L1} offers the condition for best matching of the mode width to the waveguide width: t_{L1} = 1.6 μm is our design point of reference (shaded in Table 3). The effects on the mode height are instead negligible (Mh_L ~ 0.5 μm). Also the laser stays monomodal for etch depths $t_{L1} \leq 1.6$ μm for all the widths from 2 to 6 μm and multimode for etch depths $t_{L1} > 1.6$.

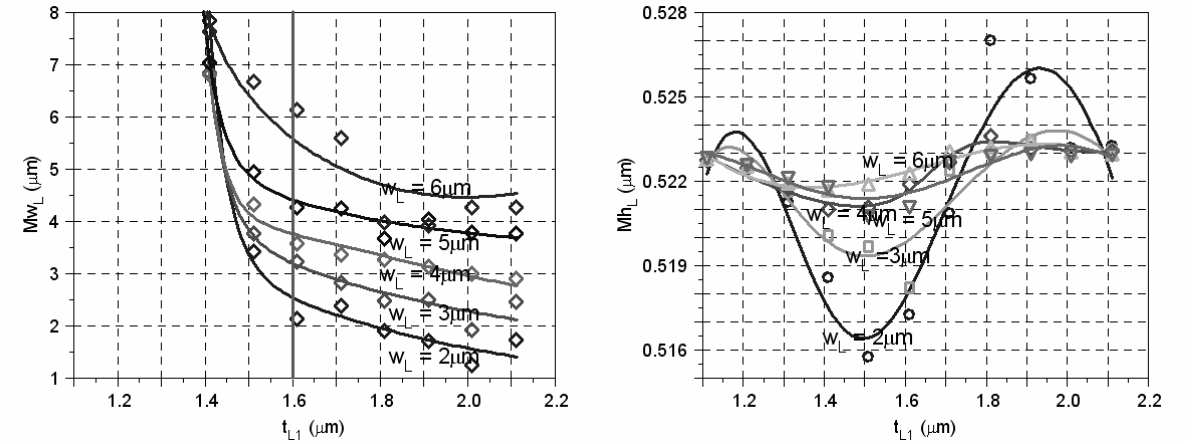

(a) (b)

Figure 4 Effect of ridge etch depth t_{L1} on the fundamental mode (a) width and (b) height for the InGaAs DQW laser waveguide.

Table 3 Mode width, Mw_L (μm) of the laser fundamental mode for several ridge widths, w_L and etch depths, t_{L1}.

w_L(μm)/ t_{L1} (μm)	1.1	1.2	1.3	1.4	1.5	1.6	1.7	1.8	1.9	2.0	2.1
2	32	28	26	7.8	3.4	2.1	2.4	1.9	1.7	1.2	1.7
3	27	26	23	6.8	3.8	3.2	2.8	2.5	2.5	1.9	2.5
4	26	24	22	6.8	4.3	3.6	3.4	3.3	3.1	3.0	2.9
5	26	24	23	7.1	4.9	4.3	4.2	3.7	4.0	3.8	3.8
6	26	24	23	7.6	6.7	6.1	5.6	4.0	3.9	4.3	4.3

In Figure 4 we show the effect of the waveguide ridge width w_W and ridge etch depth t_{W1} on the fundamental mode width for the ridge waveguide (Table 2). Values are summarized in Table 4 for convenience. For an etch depth of t_{W1} > 0.4 μm the waveguide could turn bimodal for certain widths. Therefore, an etch depth of, $t_{W1} \leq 0.4$ μm is a necessary requirement for single mode behavior. Additionally, for an etch depth of t_{W1} = 0.3-0.5 μm the mode width Mw_W is closer to the waveguide width w_W (Figure 5 (a)). For instance, as we can observe from Table 4, this happens for the waveguide ridge width of w_W = 5 & 6 μm when the etch depth is t_{W1} =0.3 μm, for a ridge width of w_W =3 & 4 μm when the etch depth is t_{W1} = 0.4 μm, and for the waveguide width of w_W = 2 μm when the etch depth is t_{W1} =0.5 μm. The narrower the waveguide a larger etch depth is required (i.e. more index contrast) to trap the energy. For an etch depth of t_{W1} ~ 0.5 μm, the mode width Mw_W has little variation for each waveguide width because the mode is totally confined within the rib.

From Figure 5 (b) we also observe that the mode height Mh_W generally stays at $Mh_W \sim 0.5$ μm, therefore the mode height of both the waveguide and laser is ~ 0.5 μm.

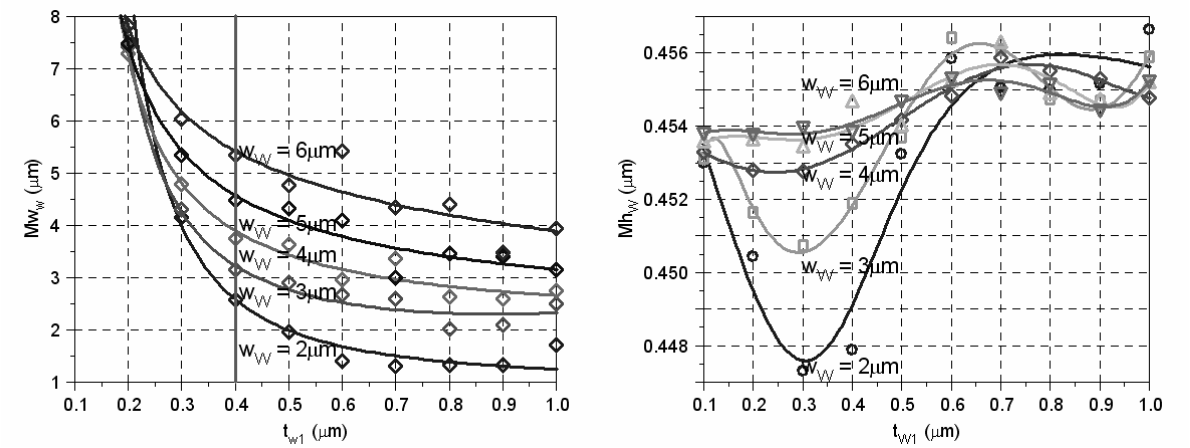

(a) (b)

Figure 5 Effect of the ridge etched depth on the width (a) and height (b) of the modes

Table 4 Mode height, Mh_W (μm) of the waveguide fundamental mode for several waveguide widths and etch depth.

w_W (μm)/ t_{W1} (μm)	0.1	0.2	0.3	0.4	0.5	0.6	0.7	0.8	0.9	1
2	55	7.3	3.8	2.5	1.9	1.8	1.6	1.4	1.6	1.4
3	20	6.3	4.0	3.1	2.7	2.5	2.3	2.5	2.4	2.1
4	14	6.3	4.5	3.8	3.7	3.6	3.5	3.3	3.2	2.9
5	12	6.8	5.2	4.8	4.5	4.2	3.5	3.8	3.4	3.3
6	12	7.2	5.9	5.5	4.7	5.5	4.7	4.3	4.5	4.5

Based on these considerations the etch depth for the laser ridge is $t_{L1} = 1.6$μm and waveguide ridge is $t_{W1} = 0.4$μm are selected in terms of best vertical and horizontal mode overlap ($Mw_L \sim Mw_W \pm 0.5$μm and $Mh_L \sim Mh_W$) while maintaining single mode operation.

We have analyzed some of the losses for the oxide waveguide (Table 5) as a function of the bottom cladding layer thickness d_W (above 1.1 μm the loss are greatly reduced). This confirms our previous slab design selection of $d_W = 1.2$ μm cladding since above it the loss becomes high.

Table 5 Waveguide fundamental mode's extinction factor κ and loss α for different bottom SiO_2 cladding thicknesses.

d_W (μm)	κ (w =2 μm)	α (dB/cm) (w =2 μm)	κ (w =4 μm)	α (dB/cm) (w=4 μm)
0.6	$3.5e^{-4}$	189	$3.3e^{-4}$	178
0.8	$6.3e^{-5}$	34	$5.3e^{-5}$	28.6
1.0	$1.2e^{-5}$	6.5	$1.16e^{-5}$	6.2
1.1	$4.7e^{-6}$	2.5	$5.6e^{-6}$	3.1
1.2	$2.2e^{-6}$	1.2	$1.6e^{-6}$	0.87
1.4	$5.6e^{-7}$	0.3	$4.2e^{-7}$	0.25

Finally, we examined the effect of waveguide core thickness on the losses, as shown in Figure 6 for ridge width, $w_W = 4$ μm. The optimum value is 0.12 μm as previously determined with the slab design, and deviations of ~0.02-0.03 μm (20-30%) would induce only < 10% reduction on the output power. Table 6 shows the design specifications for the integrated device.

Table 6 Laser and waveguide geometric dimensions defined in our design (schematic shown in Figure 3).

t_{L1}	*1.6 μm*	t_{W1}	*0.4 μm*
t_{L2}	*0.2 μm*	t_{W2}	*0.1 μm*
h_L	*0.058 μm*	h_L	*0.12 μm*
d_L	*1.85 μm*	t_L	*1.2 μm*

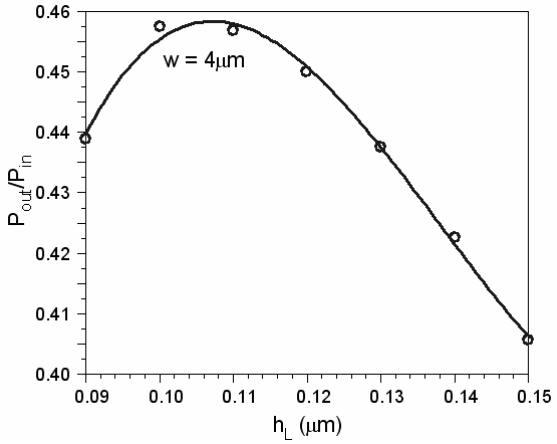

Figure 6 Output waveguide power as a function of the core thickness. A Gaussian beam was used for the input.

3. DEVICE PROCESSING AND INTEGRATION CONSIDERATIONS

The integrated laser and waveguide process relies heavily on plasma etching. The plasma etching is needed to fabricate the Fabry-Perot mirrors on the lasers which in a self aligned manner also defines the position of the waveguide [6]. We have developed a plasma etching process which results in anisotropic etching with smooth sidewalls. This is done with an electron cyclotron resonance system (ECR). The ECR system is a high ion density system (as is ICP – Inductively Coupled Plasma) where the plasma ion density is independent of the ion energy; this is in contrast to RIE (Reactive Ion Etching). ECR plasmas provide an ion density of ~ 10^{12} cm^{-2} which is 2 to 3 orders of magnitude larger than that of plasmas generated by RIE. The ion energy is provided by the DC bias across the sample plate. For RIE this is 300 to 400 V while ECR is 50 to 150 V. The high density plasma provides a large ion flux with small ion energy which yields low damage etching.

The ECR etch system is a Plasma Quest model 104 with an Astex ECR source. The maximum microwave power is 1500 W at 2.45 GHz and the maximum RF (13.56 MHz) power is 500W. The etching was optimized in terms of smooth etched morphology and vertical sidewalls, by gas composition, temperature, pressure and RF power. Using both Cl_2 (chemical etching) and Ar (sputtering) a vertical and smooth sidewall can be achieve. This is nonselective to GaAs, InGaAs and AlGaAs. The figure below shows etch chemistry for chlorine plasma for GaAs/AlGaAs/InGaAs chemical etching.

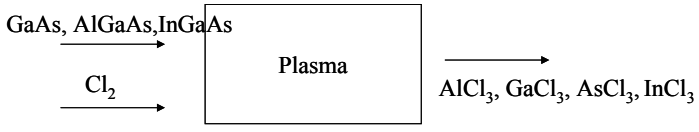

Figure 7 GaAs processing using chlorine based plasma results in highly volatile etch products.

In order to achieve smooth sidewalls in the etched GaAs, the photoresist mask must be smooth and robust. A longer ozone descum is used to "polish" the photoresist. A UV stabilization step leads to a more etch resistant photoresist mask. This works well to also suppress the lateral etching of the photoresist. Without these steps, surface striations in

the photoresist are formed which lead to sidewall striations in the etched GaAs of about 0.1 microns. However with the optimized process we have achieved sidewall roughness down to 28 Å (discussed below). Our optimized process used is as follows. The chlorine flow is 10 sccm while the Ar flow is 40 sccm. The pressure is maintained at 3 mTorr. The RF power is at 200 W and the microwave power is at 500 W. Backside helium is used to maintain a stable process temperature and the chuck is at 20 °C. Evaluation of the etching was done by scanning electron microscopy (SEM) and the etch rate was calculated by surface profilometry. The root-mean-square roughness was quantified using atomic force microscopy (AFM). The etch rate of GaAs is ~ 0.23 μm/min. The selectivity with respect to photoresist is relatively low, ~ 6. This can be increased by decreasing the argon composition. Figure 8 shows cross sectional SEM photomicrographs of the ECR etched GaAs facet with vertical etch and a smooth etched morphology. AFM images were collected using a NanoScope III Dimension 5000 (Digital Instruments, Santa Barbara, California, USA). The instrument is calibrated against a NIST traceable standard with accuracy better than 2%. NanoProbe® silicon tips were used. One 2μm x 2μm area was imaged for the top-surface sample. One 1μm x 1μm area was imaged for the sidewall scan. The AFM scans were done at Charles Evans & Associates. The AFM data is shown in Figure 9. Our surface rms roughness is 10 Å, while the sidewall roughness is 28 Å. Having smooth sidewalls on the laser mirrors is a critical requirement. Without smooth sidewalls the mirror loss will be elevated due to scattering points on the facet which will in turn decrease the light output in the lasers. With the etching described in this section we have achieved etched facet lasers that compare well to cleaved lasers showing our mirrors have very low loss; for 300 μm length and a width of 5 μm the threshold current density is ~ 10^3 A/cm^2. Etched facet lasers with various device lengths are currently under investigation to fully characterize the loss contribution from the etched facet.

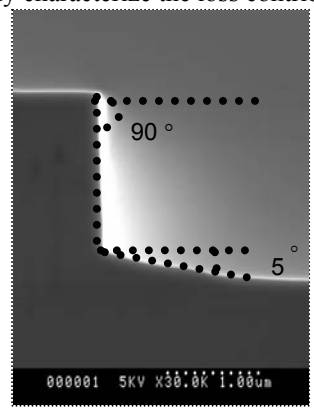

Figure 8 (a) Cross sectional SEM showing profile of ECR etched GaAs facet. Etch depth is 1.9 μm.

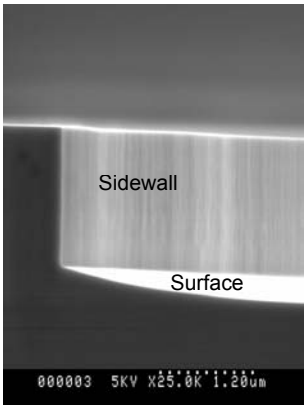

Figure 8 (b) Cross sectional SEM showing morphology of ECR etched GaAs facet. Etch depth is 1.9 μm.

Once the mirrors are defined the waveguides can be deposited in the etched mesa. This is shown schematically in Figure 1. We have investigated DC pulsed magnetron sputtering and electron beam evaporation of the SiO_2 and Ta_2O_5 layers. We found consistent low loss waveguide results with the magnetron sputtering approach, at the expense of relatively large sidewall deposition of ~ 25 %. In order to have the lowest possible loss at the laser-waveguide interface, it is desirable to have an anisotropic deposition. A smaller sidewall deposition will result in the best butt-coupling between the components. As will be discussed below; a larger gap results in additional loss. With electron beam evaporation we have been able to achieve a significant reduction in sidewall deposition, down to < 10 %. In this case, the sidewall deposition is not a continuous layer, instead a layer of pillars is formed which can be subsequently removed with a short buffered oxide etch (BOE). A representative cross-sectional SEM photomicrograph of an ebeam evaporated waveguide stack is shown in Figure 10 (a). Here you can readily see the smooth sidewall that is free of any sidewall deposition. This was possible with a 3 second BOE dip after the waveguide deposition. The core and cladding layers can also be seen from the contrast in the SEM images, an image with increased magnification is shown in figure 10 (b).

We have been able to achieve low loss waveguides using electron beam evaporation. However, we did find that it is necessary to backflow oxygen into the chamber in order to achieve SiO_2 and Ta_2O_5 that are nearly stoichiometric. Without the additional oxygen there is a deficiency in oxygen, which results in an increase in the imaginary part of the refractive index, which in turn, increases the waveguide propagation loss. The following conditions were used in order

to achieve nearly stoichiometric layers with the electron beam evaporator (base pressure $5x10^{-7}$ Torr). Oxygen was backflowed into the chamber to bring the pressure up to $5x10^{-5}$ Torr (and maintained during the evaporation) for the SiO_2 and to $1.7x10^{-4}$ for the Ta_2O_5 run. Additionally, the process temperature was set at 50 °C at the start and allowed to drift upward (source heat) to ~ 70 °C at the finish.

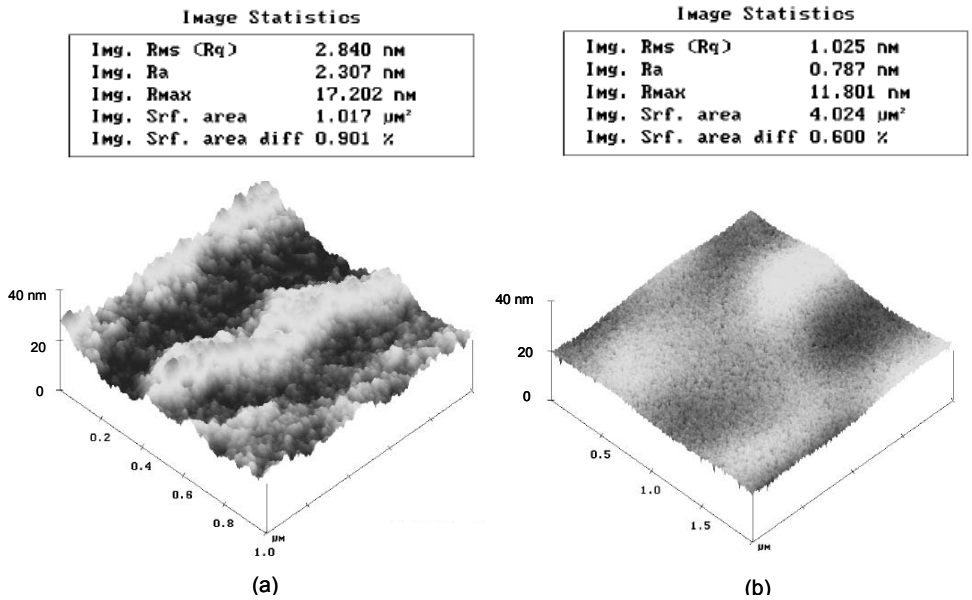

Figure 9 AFM data on GaAs with ECR etching based on Cl_2/Ar plasma. RMS roughness from (a) sidewall 28 Å and (b) surface RMS roughness of 10 Å.

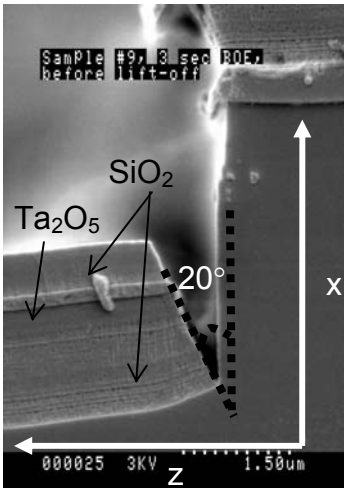

Figure 10 (a) Cross-sectional SEM image of ebeam evaporated waveguide in ECR etched GaAs trench.

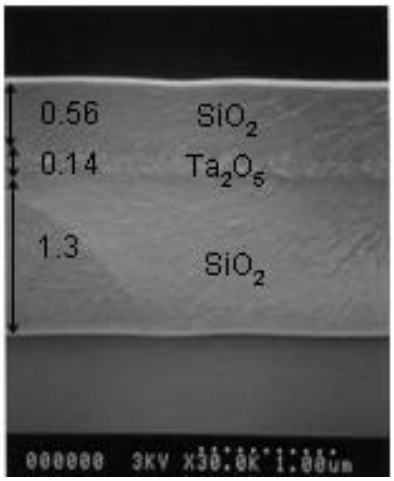

Figure 10 (b) Cross-sectional SEM image of waveguide stack. Estimated error in thickness is < 14 %.

Because of the gap, tilt, and possible offsets between the laser and the waveguide due to the fabrication processes, we analyzed numerically the effect of these parameters on the coupling behavior [7]. These are shown in Figure 11 with respect to two Cartesian systems, the $C(x,y,z)$ relative to the laser and the $C'(x', y', z')$ relative to the waveguide. In particular Δx and Δy are the vertical and horizontal offsets between the devices, Δz is the gap or end-separation, and ϕ and θ are the in-plane and out-of-plane tilting angles.

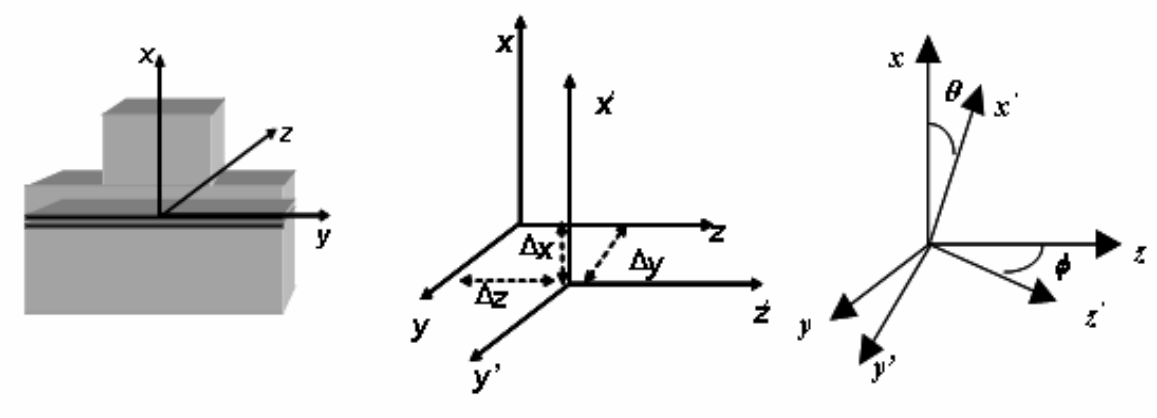

(a) **(b)** **(c)**

Figure 11. Cartesian axes $C(x,y,z)$ representing the laser and $C'(x',y',z')$ representing the waveguide. (a) Sketch of a Cartesian system relatively to a ridge waveguide. (b) Offsets Δx and Δy along transverse dimension x and y, and Δz along the propagation direction z. (c) In-plane tilt ϕ and out-of-plane θ.

We show here the results obtained by coupling a 4 μm wide laser to a 4 μm ridge waveguide, with the other geometrical dimensions defined in the previous paragraph. For instance in Figure 12 the effect of vertical offset Δx (for several values of horizontal offset Δy) between centered waveguides is shown. For vertical offset of $|\Delta x| \leq 0.15$ μm the reduction in power is ≤ 10%, whereas for a horizontal offset of $|\Delta y| \leq 1$ μm is much less critical (≤ 5%). The effect of the air-gap between the laser and the waveguides was analyzed as well. From Figure 12 (b) we can observe that for $\Delta z \leq$ 1 μm, comparable to what we observe experimentally, the power reduction is lower than 10%. Index matching fluid could be used to fill the air-gap, since this can yield an interface with less diffraction. We did not observe (via simulations) an improvement from the matching fluid, as shown in the inset of Figure 12 (b), probably because the air allows for more spreading of the mode from the laser compensating for the mismatch with the waveguide mode. We also analyzed the effect of angles with respect to the longitudinal axis z: in-plane angle ϕ (Figure 13 (a)) and out-of-plane tilt θ (in Figure 13 (b)). It can be observed that the tolerances on the angles for a power reduction of ~10% are $\phi \leq$ 2.0°, and $\theta \leq$ 9.0°. For the working condition of θ ~20° the power reduction is ~ 27 %. (dotted line in Figure 13 (b)). The out-of-plane tilt, θ is the most significant loss mechanism for our integrated device. Further process optimization is needed to reduce the tilt which can clearly be seen from Figure 10a. The photoresist mask which defines the etched mirror facet, and in a self-aligned manner also defines the region for the waveguide deposition, is responsible for shadowing the evaporated dielectric waveguide. Therefore, the mask or waveguide process needs to be improved in order to decrease this loss.

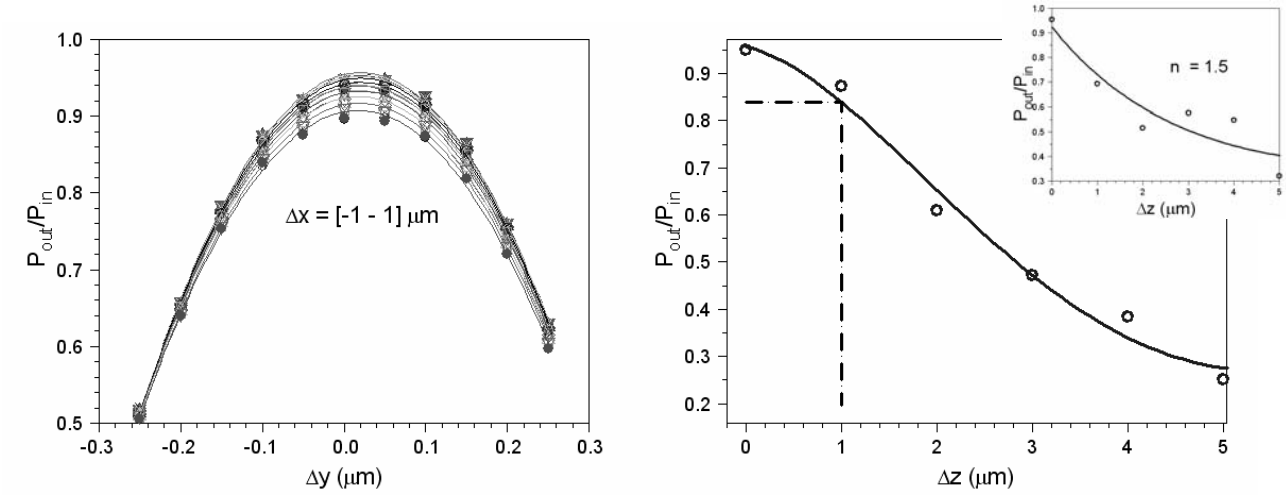

(a) (b)

Figure 12 Effect of (a) Δx for several values of Δy and (b) Δz between butt-coupled waveguides (w = 4 μm).

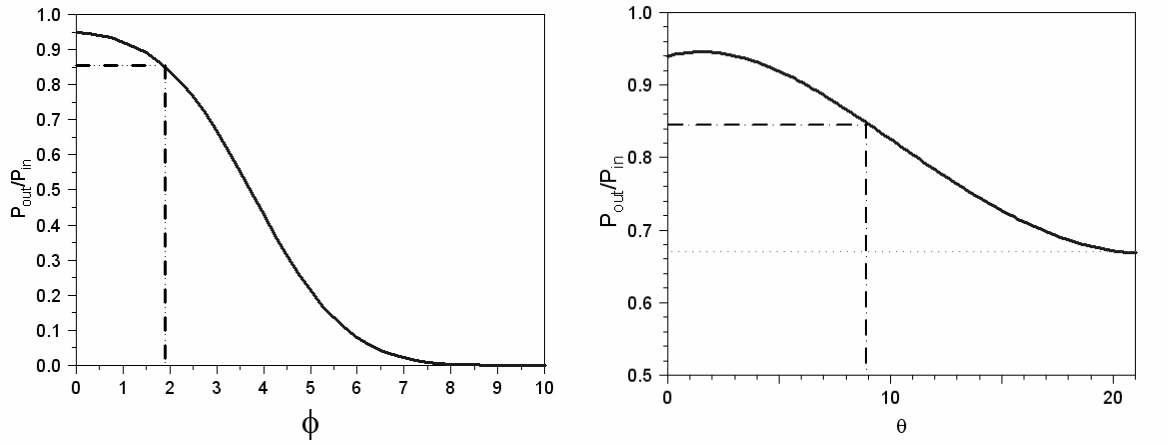

(a) (b)

Figure 13 Output power from the waveguide (w= 4 μm) after launching the (w=4 μm) laser mode for (a) in-plane and (b) out-of-plane tilt between the laser and the waveguide.

4. MEASUREMENTS

The integrated laser-waveguide system has been measured in terms of current versus output optical power. Figure 14 shows the top view of the integrated device showing the position of the etched facet laser and dielectric waveguides. A cantilever probe was applied to the p metal contact and a constant current source was used. The light is detected with a standard silicon detector. Figure 14b shows a top view of a representative device under test. Figure 15 shows the performance of the integrated laser-waveguide device. The output is taken on one of the laser facets only. The laser length is 300 μm while the waveguide is 17.5 μm long. The slope efficiency of the integrated device is as high as 0.45 W/A (from a single facet). It should be pointed out that in the current configuration the waveguide is only confined in the vertical direction (broad area waveguide). We expect to achieve even higher efficiency when the waveguide mode is confined in both the vertical and horizontal directions. This will be done with a ridge etch on the SiO_2. Waveguides with this structure and cross section as shown in Table 2 and Figure 3 (b) were fabricated and resulted in low loss waveguides with loss below 3 dB/cm, as shown in Figure 16. We are currently fabricating an integrated laser-waveguide device with ridge widths of 4 μm (both laser and waveguide) to achieve single mode behavior in both devices.

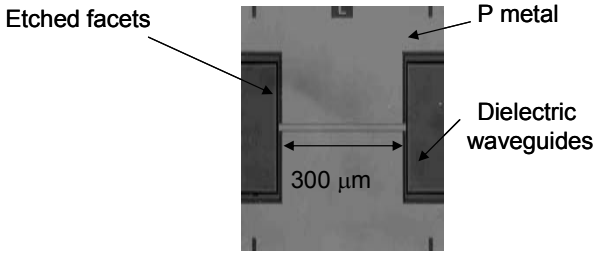

Figure 14 (a) Top view of integrated laser-waveguide device.

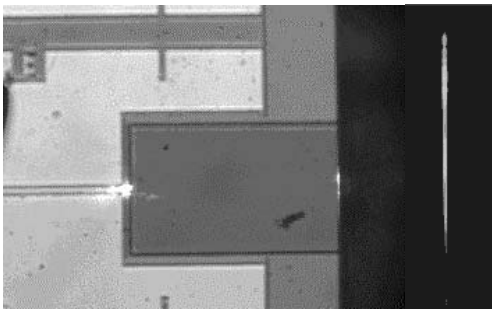

Figure 14 (b) Top-view of the laser butt coupled to broad area waveguide (left) with CCD camera, view of the output light through the coupled devices.

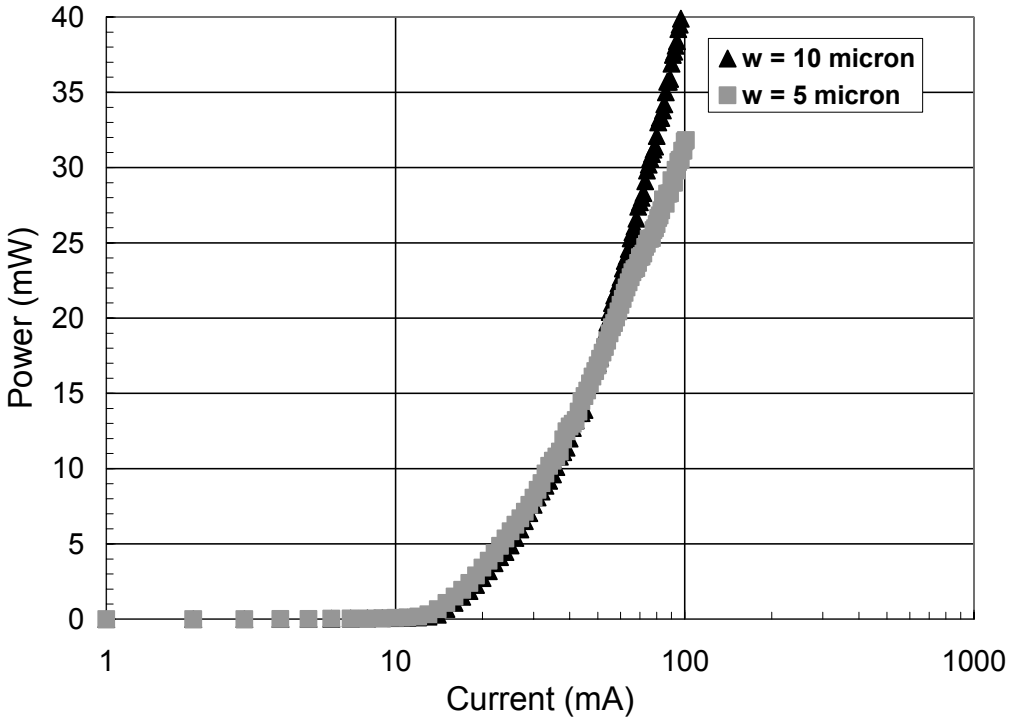

Figure 15 Optical power versus current for the integrated laser-waveguide device.
Laser length = 300 μm, waveguide length = 17.5 μm.

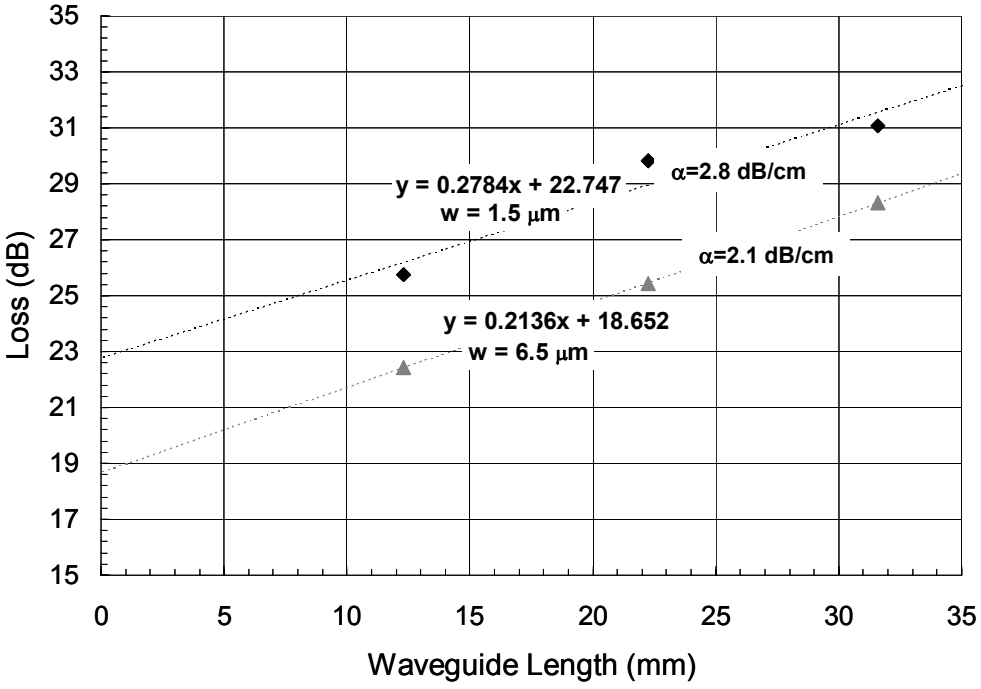

Figure 16 Cut-back measurement data of $SiO_2/Ta_2O_5/SiO_2$ waveguides.

5. CONCLUSION

We have developed a methodology to integrate dielectric waveguides and etched facet lasers in a planar configuration. The design of this integrated device is based on the evaluation of the optical mode in each component and tailoring the mode in terms of mode height and width by modifying the etch depth. By modifying the etch depth in both the laser and waveguide device we show that the mode overlap can be better than 90 %. In the butt coupled EEL/waveguide system we have measured a slope efficiency to be as high as 0.45 W/A. The effects of the waveguide transmission loss, alignment error, air gap spacing and tilt between the laser and waveguide have been quantified. For the current configuration of Δz=1μm air gap (between the laser and waveguide) and out-of-plane tilt θ~20°, the estimated additional loss due to alignment errors is roughly 3dB. This interconnect loss is low, however we believe this can be further reduced by advancing our waveguide deposition process. In conclusion we have demonstrated a technology that allows direct coupling of a dielectric optical interconnect to a semiconductor laser monolithically fabricated on the semiconductor substrate.

REFERENCES

1. M. Takenaka and Y. Nakano, "First Realization of All-Optical Flip-Flop Based on Bistable Laser Diode with Active Multimode Interference Cavity," *OFC 2004 Proceedings, paper WL4*.
2. G.A. Vawter, C. Alford, G. Peake, F. Cajas, B. Salters, J. Wendt and W. Zubrzycki, "Monolithic-integrated Optical Gain Competition Inverter," *IPR 2004 Proceedings, paper IthB5*.
3. H.S. Djie, T. Mei, J. Arokiaraj and D. Nie, "Single Step Quantum Well Intermixing with Multiple Band Gap Control for III-V Compound Semiconductors," *Journal of. Applied Physics*, vol. **96**, no. 6, pp.3282-5, 2004.
4. D.P. Prakash, D.C. Scott, H.R. Fetterman, M. Matloubian, Q. Du and W. Wang, "Integration of Polyimide Waveguides with Traveling-Wave Phototransistors," *IEEE Photonics Technology Letters*, vol. **9**, no. 6, pp. 800-802, 1997.
5. T. Nakahara, H. Tsuda, K. Tateno, S. Matsuo and T. Kurokawa, "Hybrid Integration of Smart Pixels by Using Polymide Bonding: Demonstration of a GaAs Photodiode/CMOS Reciever," *IEEE Journal of Selected Topics in Quantum Electronics*, vol. **5**, no.2 , pp.209-16, 1999.
6. A. Behfar-Rad, S.S. Wong, J.M. Ballantyne, B.A. Soltz and C.M. Harding, "Rectangular and L-shaped GaAs/AlGaAs Lasers with Very High Quality Etched Facets," *Applied Physics Letters*, vol. **54**, no.6, pp. 493-5, 1989.
7. D. Marcuse, "Tilt, offset, and end-separation loss of lowest-order slab waveguide mode", *Journal of Lightwave Technology*, vol. **4**, no. 11, p. 1647-1650, 1986.

This work was performed under the auspices of the U.S. Department of Energy by University of California, Lawrence Livermore National Laboratory under Contract W-7405-Eng-48.